A&A 491, 789–796 (2008)
DOI: 10.1051/0004-6361:200810089

Astronomy & Astrophysics

H I and CO in the circumstellar environment of the oxygen-rich AGB star RX Leporis

Y. Libert[1], T. Le Bertre[1], E. Gérard[2], and J. M. Winters[3]

[1] LERMA, UMR 8112, Observatoire de Paris, 61 Av. de l'Observatoire, 75014 Paris, France
e-mail: yannick.libert@obspm.fr
[2] GEPI, UMR 8111, Observatoire de Paris, 5 place J. Janssen, 92195 Meudon Cedex, France
[3] IRAM, 300 rue de la Piscine, 38406 St. Martin d'Hères, France

Received 29 April 2008 / Accepted 21 August 2008

ABSTRACT

Context. Circumstellar shells around AGB stars are built over long periods of time that may reach several million years. They may therefore be extended over large sizes (~1 pc, possibly more), and different complementary tracers are needed to describe their global properties.
Aims. We set up a program to explore the properties of matter in the external parts of circumstellar shells around AGB stars and to relate them to those of the central sources (inner shells and stellar atmospheres).
Methods. In the present work, we combined 21-cm H I and CO rotational line data obtained on an oxygen-rich semi-regular variable, RX Lep, to describe the global properties of its circumstellar environment.
Results. With the SEST, we detected the CO(2–1) rotational line from RX Lep. The line profile is parabolic and implies an expansion velocity of ~4.2 km s^{-1} and a mass-loss rate ~1.7×10^{-7} $M_\odot$ yr^{-1} (d = 137 pc). The H I line at 21 cm was detected with the Nançay Radiotelescope on the star position and at several offset positions. The linear shell size is relatively small, ~0.1 pc, but we detect a trail extending southward to ~0.5 pc. The line profiles are approximately Gaussian with an $FWHM$ ~ 3.8 km s^{-1} and interpreted with a model developed for the detached shell around the carbon-rich AGB star Y CVn. Our H I spectra are well-reproduced by assuming a constant outflow ($\dot{M}$ = 1.65×10^{-7} $M_\odot$ yr^{-1}) of ~4×10^4 years duration, which has been slowed down by the external medium. The spatial offset of the H I source is consistent with the northward direction of the proper motion measured by Hipparcos, lending support to the presence of a trail resulting from the motion of the source through the ISM, as already suggested for Mira, RS Cnc, and other sources detected in H I . The source was also observed in SiO (3 mm) and OH (18 cm), but not detected.
Conclusions. A detached shell, similar to the one around Y CVn, was discovered in H I around RX Lep. We also found evidence of an extension in the direction opposite to the star proper motion. The properties of the external parts of circumstellar shells around AGB stars should be dominated by the interaction between stellar outflows and external matter for oxygen-rich, as well as for carbon-rich, sources, and the 21-cm H I line provides a very useful tracer of these regions.

Key words. stars: individual: RX Lep – stars: mass-loss – stars: AGB and post-AGB – stars: winds, outflows – radio lines: stars – stars: circumstellar matter

1. Introduction

Evolved stars on the asymptotic giant branch (AGB) are often surrounded by circumstellar shells. The material in these shells is flowing outwards with velocities from a few km s^{-1} up to 40 km s^{-1} (Nyman et al. 1992). The observed mass-loss rates range from ~10^{-8} to a few 10^{-4} $M_\odot$ yr^{-1} (e.g. Knapp & Morris 1985; Olofsson et al. 2002), the lower limit being probably set by detectability. In this phase of the stellar life, the evolution is dominated by mass loss rather than nuclear processes (Olofsson 1999). The history of mass loss over the full AGB is complex and the details of this process are currently not well known (e.g., Lafon & Berruyer 1991; Habing 1996; Leão et al. 2006). A general picture, however, has arisen from both theoretical and observational findings that – on average – the mass-loss rate increases towards the end of the AGB phase, leading in some cases to the formation of a planetary nebula (e.g., Renzini 1981; Hrivnak & Bieging 2005).

The validity of this simple picture may depend on the parameters of the star, e.g., on its initial mass. Schröder et al. (1999) combine mass-loss rates derived from consistent wind models with stellar evolution calculations and find that the mass-loss rate should increase along the AGB for stars with initial masses greater than 1.3 $M_\odot$. Stars with lower initial mass would experience a single short-lived (~1000 yr) episode of high mass loss only, which would leave behind a very narrow detached shell as observed in the case of, e.g., TT Cyg (Olofsson et al. 2000). On the other hand, the mass-loss phenomenon appears to be highly variable on even shorter time scales as indicated e.g. by concentric arcs observed in scattered light around the prototype carbon Mira IRC +10216 (Mauron & Huggins 2000) and around some proto-planetary nebulae (e.g., Hrivnak et al. 2001). The time scale of these mass-loss variations would be around a few 10^2 yr. The physical mechanism responsible for these variations still needs to be identified, although different possibilities have already been proposed: e.g., interaction between gas and dust within stellar outflows (Simis et al. 2001), or solar-like magnetic cycle (Soker 2002). In contrast to these later phases of AGB mass loss at rather high rates (~10^{-5} $M_\odot$ yr^{-1}), information about the mass-loss process on the early AGB, is even scarcer.

To unravel the processes involved in the mass-loss phenomenon, we have to find suitable tracers. One of the most

studied among these tracers is the CO molecule, because so far it has been considered to provide the best estimate of the mass-loss rate for AGB stars (Ramstedt et al. 2008). Not only can it be used to estimate this mass-loss rate, but it also yields important parameters of the AGB wind (e.g.: expansion velocity, central star velocity, etc.). Since CO is photodissociated by UV radiation from the interstellar radiation field (ISRF), it can only probe the inner parts ($r \leq 10^{-3}$–10^{-1} pc, Mamon et al. 1988) of circumstellar shells (CSs). Therefore, the CO emission is only related to "recent" (i.e. a few 10^3–10^4 years) mass-loss episodes.

On the other hand, H I is in general protected from photoionization by the surrounding interstellar medium (ISM). As a result, H I can be used to probe the external parts of circumstellar shells and can give indications on the mass-loss on longer timescales (a few 10^5 years: Libert et al. 2007). Hence, CO and H I complement each other nicely to describe the history of the mass-loss rate of an AGB star.

The drawbacks of H I circumstellar observations are that hydrogen is ubiquitous in the Galaxy and that the genuine stellar H I must be separated from the ambient H I. Ideal cases would be bright H I sources, with relatively high velocity with respect to the local standard of rest (LSR) and reasonably far above the Galactic plane. For the other sources, the interstellar H I should be studied with care. In the present paper, we analyze this confusion with a new approach that consists in a 3D-mapping using H I spectra.

The mass-loss phenomenon is different from one AGB star to another and may vary highly with time. Nevertheless, observing in H I provides a global view of the CS behavior and, on timescales of about 10^5 years, small variations in the mass-loss rate may be flattened out. Thus, we have developed a model of the circumstellar gas, based on a scenario already proposed by Young et al. (1993), in which CSs are the result of a constant outflow eventually slowed down by the surrounding medium. This deceleration produces a snowplough effect around the source, resulting in a detached shell of compressed matter originating from the star and the external medium (Lamers & Cassinelli 1999, Chap. 12).

A schematic view of this model can be pictured as follows: a wind is flowing outward from the star, in free expansion with a constant velocity ($V_{\rm exp}$) and a constant rate. It encounters a shock at a radius r_1 (termination shock), due to the slowing down by the surrounding matter. Between r_1 and $r_{\rm f}$ (contact discontinuity), the stellar matter is compressed. Between $r_{\rm f}$ and until a second shock at r_2 (bow shock), the interstellar matter has been swept up by the wind of the AGB star. Finally, beyond r_2, the external matter is considered to be at rest.

Recently, we successfully applied this model to a carbon-rich star: Y CVn (Libert et al. 2007). In H I at 21 cm, this star exhibits a composite profile, made of a broad, rectangular component and a narrow, Gaussian-shaped one. In our description, the broad component is the signature of the freely expanding wind, whereas the narrow component is produced by the H I compressed in the snowplough between r_1 and r_2. Our model provides a simple explanation for some of the so-called "detached dust shells" observed in the far infrared (Izumiura et al. 1996). If this approach is correct, then it should also apply to detached shells around oxygen-rich AGB stars. In this paper we present H I and CO data that we obtained on an oxygen-rich AGB star, RX Lep, and interpret them with the model that we developed for Y CVn. The H I interstellar confusion in the direction of RX Lep is moderate and we illustrate, in that case, our new approach to extract a genuine H I spectrum.

In this simplified description we assume spherical symmetry. However, recent H I, far-infrared and UV data (Gérard & Le Bertre 2006; Matthews & Reid 2007; Ueta et al. 2006; Martin et al. 2007) have shown that the AGB star motion with respect to the ISM may lead to a distortion, and eventually a disruption, of the circumstellar environment. Previous, and more recent, numerical modelings (Villaver et al. 2003; Wareing et al. 2007) are in line with this interpretation. The circumstellar environment of RX Lep might provide a new illustration of this phenomenon, and we will discuss this possibility.

2. RX Lep

RX Lep has been classified as an irregular variable, Lb star (General Catalogue of Variable Stars, GCVS 3rd edn., Kukarkin et al. 1971). A photometric monitoring over 8 years shows variations of about ±1 mag in the V band (Cristian et al. 1995). The periodogram analysis gives a main period in the range 80–100 days and a possible secondary period around 60 days. Recently, the star has been re-assigned to the type SRb (GCVS 4.2, Samus et al. 2004), because it may exhibit a periodic variability of a few tenths of a magnitude.

The Hipparcos parallax (7.30 ± 0.71 mas) places the star at 137^{+15}_{-12} pc from the Sun and at ~65 pc away from the Galactic plane ($b^{\rm II} = -27.51°$). The proper motion, also given by Hipparcos, is 31.76 ± 0.58 mas yr^{-1} in right ascension (RA) and 56.93 ± 0.50 mas yr^{-1} in declination (Dec). At 137 pc, it translates into a motion in the plane of the sky of 44 km s^{-1} (corrected for solar motion, as determined by Dehnen & Binney 1998) in the northeast direction (PA ~ 31°).

Fouqué et al. (1992) have obtained near-infrared photometry data and, using the bolometric correction of Le Bertre et al. (2001), we derived a luminosity of 4500 $L_\odot$. This luminosity confirms that RX Lep is on the AGB. The effective temperature is ~3300 K (Dumm & Schild 1998). This means that hydrogen is expected to already be mostly in atomic form in the atmosphere and throughout the CS (Glassgold & Huggins 1983). Technetium lines (^{99}Tc) were searched for in the 4200–4300 Å region and not detected (Lebzelter & Hron 1999), confirming an older result from Little et al. (1987). This tends to indicate that RX Lep has not gone through a thermal pulse and that it is still in the early phase of the AGB (E-AGB). This is in good agreement with the results of Mennessier et al. (2001) who, using astrometric and kinematic data, place RX Lep among E-AGB stars that belong to the Galactic disk population with initial masses in the range 2.5–4 $M_\odot$.

Paschenko et al. (1971) did not detect the source in the OH satellite line at 1612 MHz. As this is the only OH observation reported in the literature, we observed RX Lep again at 18 cm on Jan. 12, 2006 and July 14, 2006 with the NRT. No emission was detected at a level of 0.015 Jy in any of the 4 OH lines (1612, 1665, 1667, and 1720 MHz).

RX Lep might be associated with an IRAS extended source (X0509-119, IRAS Science Team 1988) at 60 (diameter ~1.1′) and 100 μm (diameter ~6.0′). However, X0509-119 is centered at about 2.5′ east from RX Lep, and that association might only be fortuitous. We present a re-analysis of the IRAS results farther down (Sect. 6).

Kerschbaum & Olofsson (1999) report a CO (1–0) and CO (2–1) detection, but their radial velocity is doubtful: $v_{\rm hel}$ ~ 29 km s^{-1} (as compared to $v_{\rm hel}$ ~ 46 km s^{-1} cited in the General Catalogue of Stellar Radial Velocities, GCRV, Wilson 1953). Our new results (Sect. 3) now suggest there has likely

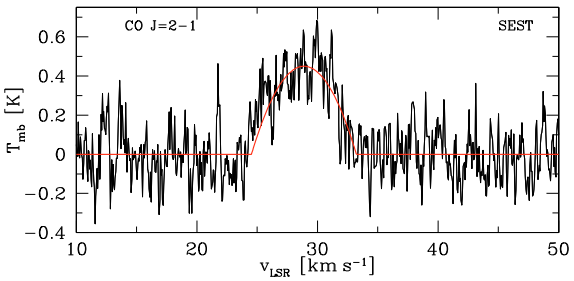

Fig. 1. CO (2–1) emission of RX Lep. The solid line represents a parabolic fit (Sect. 3).

been a confusion between the heliocentric and LSR reference frames.

3. Molecular line observations

RX Lep was part of a CO observing program dedicated to the Valinhos "*b*" class stars (Epchtein et al. 1987). This class of sources is defined by a weak near-IR excess as compared with the IRAS fluxes ($0.2 < K - L' < 0.7$ and $0.8 < L' - [12] < 2$). The central stars are generally identified with late-M giants surrounded by tenuous circumstellar shells. Those stars were suspected by Winters et al. (2000) to show preferentially low expansion velocity winds. Most of the data from this program have been published in Winters et al. (2003). Subsequently, RX Lep's CO (2–1) emission at 230 GHz and SiO ($v = 1$, $J = 2$–1) maser transition at 86 GHz have been searched using the 15-m Swedish-ESO Submillimetre Telescope, SEST (Booth et al. 1989) on January 30, 2003. At 1.3 mm, the *FWHM* of the SEST beam is 23″. We used the position-switch mode with a beam throw of 11.5′. The spectra were recorded on the high-resolution spectrometer (HRS) giving a resolution of 80 kHz, for a channel separation of 43 kHz and a bandwidth of 86 MHz.

The CO (2–1) transition was clearly detected (Fig. 1). The resulting profile was fitted with a parabolic curve, and we derived an LSR velocity of $V_{\rm lsr} = 28.9 \pm 0.1$ km s^{-1}, an expansion velocity of $V_{\rm exp} = 4.2 \pm 0.1$ km s^{-1}, and an amplitude of $T_{\rm mb} = 0.45\,{\rm K} \pm 0.13$ K. By using the same method as Winters et al. (2003, Sect. 4.3), we estimated both RX Lep mass-loss rate and CO photo-dissociation radius using the results of the line fitting. We find $\dot{M} \sim 1.7 \times 10^{-7}\ M_\odot$ yr^{-1} and $r_{\rm CO} \sim 0.8 \times 10^{-2}$ pc (≡12.5″). On the other hand, the SiO maser was not detected at a level of 0.2 Jy.

Our CO measurement of the LSR radial velocity (28.9 km s^{-1}) is consistent with the heliocentric velocity quoted in the GCRV. Combining this result with the Hipparcos determination of the velocity in the plane of the sky (44 km s^{-1}), we get a 3D space velocity of 53 km s^{-1}.

4. H I observations

RX Lep has been observed during a total of 141 h between February 2005 and February 2008 with the Nançay Radiotelescope (NRT). The NRT is a meridian telescope with a rectangular aperture of effective dimensions 160 × 30 m. At 21 cm and at the declination of RX Lep, the *FWHM* of the beam is 4′ in RA and 22′ in declination. We used the position-switch technique with two off-positions in the east-west direction, every 2′, and up to 24′ from the source. Thus, the total time spent on-source was 47 h. To fully describe the environment of RX Lep, we sampled our map every half beam in RA and in Dec (hereafter, the position-switch spectra will be referred to as

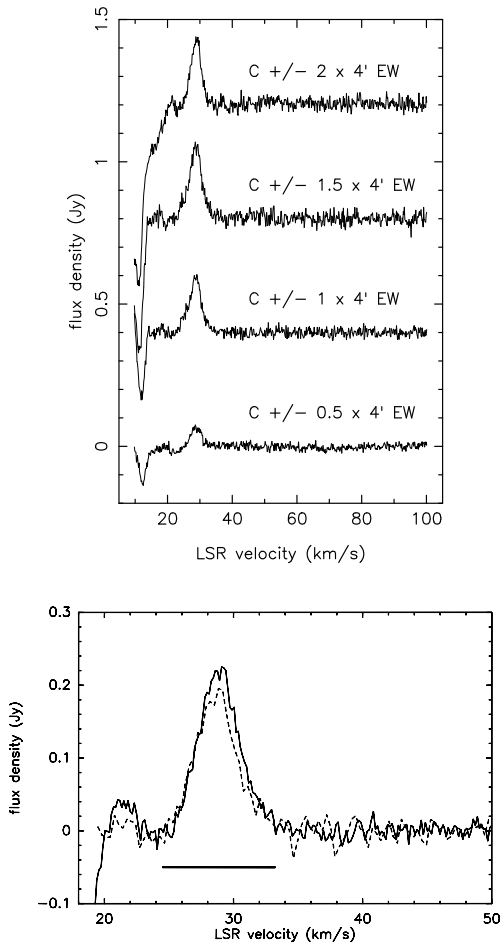

Fig. 2. *Upper panel*: spectra obtained in position-switch mode with the NRT. The positions are expressed in number of beams (4′). The maximum intensity is reached at C ± 1.5 × 4′ EW. For clarity, the individual spectra have been displayed with vertical offsets of 0.4 Jy. *Lower panel*: average spectrum computed with C ± n × 4′ EW, $n > 1.5$. Dotted line: baseline subtracted f-switch spectrum. The horizontal line shows the width of the CO signal.

C ± n × 4′ EW, n being the number of beams for the off positions). At 21 cm, the spectra have a bandwidth of 165 km s^{-1} and a channel width of 0.08 km s^{-1}. For convenient analysis, we smoothed the data with a Hanning filter so that the spectral resolution was 0.16 km s^{-1}. The data are processed with the CLASS software, part of the GILDAS[1] package developed at IRAM (Pety 2005).

The different steps of the data processing can be described as follows. First of all, we determine the spatial extent of the source by comparing the C ± n × 4′ EW spectra. When the maximum intensity of the peak is reached ($n = n_{\rm max}$), the source does not contribute to the flux of the offset spectra anymore. For example, according to Fig. 2 (upper panel), RX Lep does not extend farther than 6′ in the E-W direction. Once the maximum extent is estimated, the average of the C ± n × 4′ EW spectra with $n > n_{\rm max}$ gives the central spectrum (Fig. 2, lower panel). Simple arithmetic then allows to extract the spectra at the offset positions, using the central spectrum.

We present a new visualization of the H I spectra to better separate the genuine stellar H I from the contamination due to interstellar hydrogen. The operation can be described as a

[1] http://www.iram.fr/IRAMFR/GILDAS

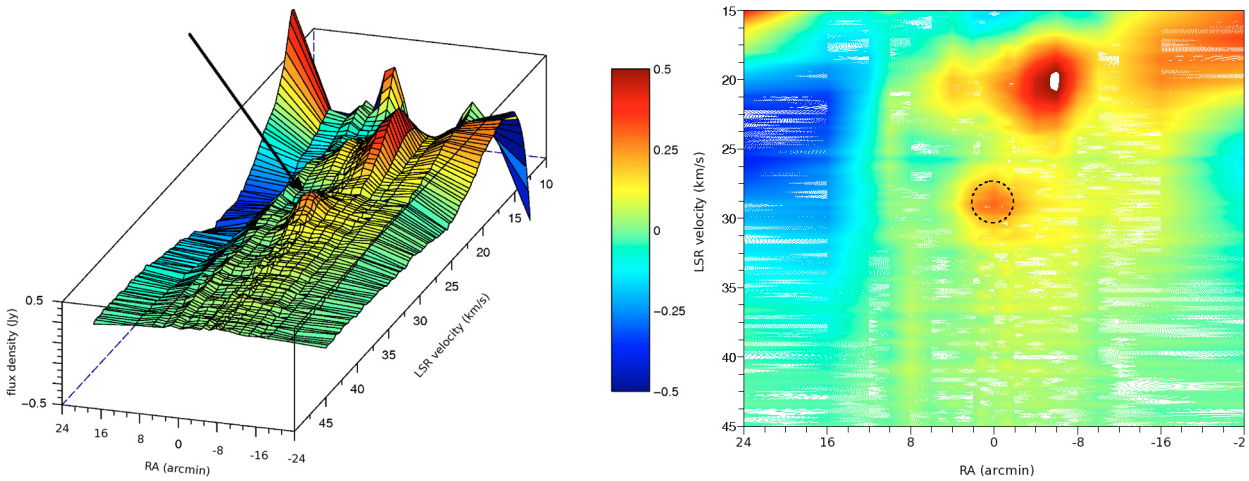

Fig. 3. *Left panel*: 3D velocity-position representation of the H I flux density; east is to the left. The arrow points to the expected position of the source. *Right panel*: the same data set represented in 2D; west is to the right. The dashed circle surrounds the expected position of RX Lep.

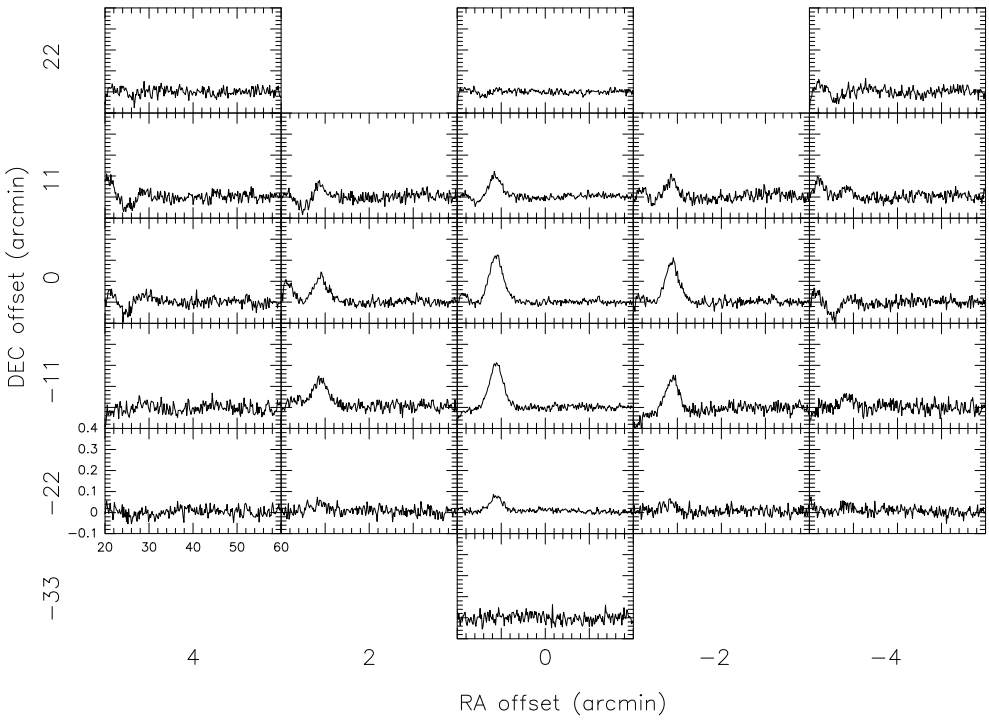

Fig. 4. H I map of RX Lep. The steps are 2′ in RA and 11′ in Dec. The positions are indicated with respect to the stellar position. The abscissae and ordinates are LSR radial velocities (km s^{-1}) and flux densities (Jy) as indicated on the lower left corner.

stacking of the NRT spectra, processed as above, in the east-west direction, for a given declination (Fig. 3). In this view, velocity is given as a function of right ascension, and intensity is represented using a colored scale. This aims at visualizing, and thus separating, the H I emission coming from the source and that from the Galaxy. Indeed, on the resulting image, the stellar H I should be nearly centered in RA and close to the LSR velocity given by CO observations. While this process emphasizes the difficulties coming from the contamination due to the Galactic hydrogen emission, it also allows an evaluation of the possible problems when processing the data and a design of the best strategy for extracting the intrinsic source emission.

According to Fig. 3, RX Lep is definitely a suitable candidate for H I observation, as it is clearly separated from the interstellar emission spectrally and spatially, although the confusion increases for velocities lower than 29 km s^{-1}. Indeed, the image shows 2 potential sources of contamination: one around 4′W from the source and at ∼20 km s^{-1}, the other increasing (negatively) at 16′E and around 24 km s^{-1}. This information is crucial to safely extracting the intrinsic emission of RX Lep. Thus, to build the map of the source, we fitted polynomial baselines (in some cases of degree up to 3 when the confusion reaches its highest level) to a portion of the spectrum between 21 and 54 km s^{-1}. The resulting map of RX Lep is shown in Fig. 4.

We independently confirmed these results by observing the source using the frequency-switch mode (Fig. 2, lower panel). We spent 5 h on source and detected it at the same velocity and with the same flux density as shown on the map for the central position.

From our observations, we can readily derive some important properties of the CS. The map of RX Lep in Fig. 4 reveals that the H I line profile, at the central position, shows a quasi-Gaussian shape of central velocity 28.84 ± 0.03 km s^{-1}, *FWHM* 3.8 ± 0.1 km s^{-1}, and flux density 0.22 ± 0.03 Jy. The shape

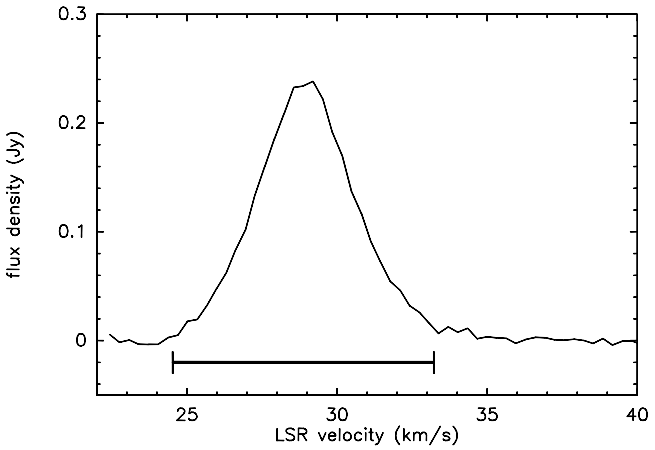

Fig. 5. Average of the spectra C ± n × 4′ EW and 11′S ± n × 4′ EW with $n > 1$. The horizontal line represents the width of the CO line.

of this line differs from that of the parabolic CO line. It clearly indicates a slowing down of the wind within the outer parts of the CS (Le Bertre & Gérard 2004). Moreover, assuming that the broadening of the H I emission line is dominated by the thermal Doppler effect, the *FWHM* of the spectrum allows us to estimate an upper limit to the average temperature in the shell (Libert et al. 2007, Eq. (1)). It gives us $T_{\rm mean} < 312$ K.

Evidence of a composite line profile such as that of Y CVn (Sect. 1) is difficult to see, given the fairly low intensity of the signal and the narrow width of the expected pedestal ($2 \times V_{\rm exp}$). Nevertheless, from the central spectrum, we can set an upper limit to the amplitude of a possible pedestal. We estimate this limit at 20 mJy by assuming it has the same width as the CO profile (Fig. 5).

The map of RX Lep (Fig. 4) shows that the H I brightness distribution of the envelope is offset from the stellar position both in RA and Dec. There is a slight westward RA offset <1′ (since the flux density at 2′ west is larger than at 2′ east but smaller than at the center). There is a southward Dec. offset close to 5.5′ (since the flux density at 11′ south is nearly equal to the central flux). It is useful to give quantitative estimates, not only of the offsets but also of the spatial extents for the model calculations that will be discussed in Sect. 5. If one assumes that the H I brightness distribution is Gaussian in RA (and Dec) and offset, the convolution by a Gaussian beam also produces a Gaussian distribution and one can retrieve from the data both the offset and half power width (HPW) in RA (and Dec). The RA offset and HPW are respectively −0.4′ (±0.2′) and 2.3′ (±0.5′). The Dec offset and HPW are respectively −4.4′ (±0.6′) and 15′ (±3′). Thus the H I envelope is elongated southwards and offset from the stellar position by 4.4′ at PA 185° (i.e. also nearly southward). This suggests an HI envelope trailing south.

The integrated flux throughout the map gives 1.22 Jy × km s^{-1}, which translates into a hydrogen mass of $\sim 5.42 \times 10^{-3}$ $M_\odot$ (assuming no hydrogen in H_2; cf. Sect. 2). Adopting a mean molecular weight of 1.3, it translates into a total mass of the gas in the shell of $\sim 7.05 \times 10^{-3}$ $M_\odot$. If we consider the mass-loss rate to be constant and adopt the estimate given by CO, then the age of the CS is ∼42 700 years, about one order of magnitude less than the age we estimated for Y CVn.

5. Model

The high-quality H I spectral profiles that we have obtained in the direction of RX Lep are similar to those of Y CVn (Libert et al. 2007). This type of profile is indicative of a slowing-down of stellar outflows in the external parts of CSs (Le Bertre & Gérard 2004). In the following we apply the model that we developed for the carbon-rich star Y CVn in order to evaluate the physical conditions within the shell of RX Lep. Of course, as this model assumes sphericity, it cannot reproduce the more complex geometry suggested by the map presented in the previous section. In the east-west direction the map is fairly symmetric, so the model could apply. However, there is also a clear north-south extension that would require a 2D model, as well as a spatial resolution better than 22′ (the NRT beam).

A 1D-hydrodynamic code provides the density distribution within the detached shell based on the hypothesis of a slowing down of the stellar gas by the surrounding local material. The mass-loss rate is constant, and the gas expanding outward from the atmosphere is in free expansion with a constant velocity $V_{\rm exp}$. Then, the outflow encounters a shock (r_1). Its velocity decreases by a factor of about 4 and the matter keeps on decelerating until it reaches the external medium (at $r_{\rm f}$). The external matter that has been swept up and compressed by the expansion of the stellar envelope lies outside $r_{\rm f}$. Finally, beyond r_2, the gas is at rest.

The expansion velocity and the LSR velocity of the source are based on the results from our CO observations. But RX Lep has not been studied much, so we lack some spatial information such as estimates of r_1 and r_2 that could have been obtained, for example, with dust continuum observations. Nevertheless, the NRT map indicates that the object is fairly small in the east/west direction (∼2.3′ i.e. $\sim 9 \times 10^{-2}$ pc at 137 pc).

One of the results of our model is that detached shells are flagged by a composite H I spectrum. The first component (Comp. 1) is narrow, with a quasi-Gaussian shape and it arises from the matter slowed down by the local medium. The second component (Comp. 2) is broad with a rectangular shape, as it probes the inner part of the shell where the gas is in free expansion. In Sect. 4, we set an upper limit of Comp. 2 of ∼20 mJy. For a constant mass-loss rate, we can derive a relation (Eq. (1)) to estimate r_1:

$$r_1 \approx 2.17 \times 10^{-9} \times \frac{d\, V_{\rm exp}^2\, F_{\rm Comp.2}}{\dot{M}} \qquad (1)$$

where r_1 is expressed in arcmin, d is the distance in pc, $V_{\rm exp}$ is in km s^{-1}, $F_{\rm Comp.2}$ is the intensity of the pedestal in Jy, and $\dot{M}$ is in $M_\odot$ yr^{-1}. With $V_{\rm exp} = 4.2$ km s^{-1} and $\dot{M} = 1.65 \times 10^{-7}$ $M_\odot$ yr^{-1} (Sect. 3), we estimate an upper limit for r_1 of 0.64′. We set r_2 at 1.15′, in agreement with the H I observations in the east-west direction (HPW/2, Sect. 4).

As our model assumes spherical symmetry, we performed a fitting on a symmetrized map, i.e. a map in which the offset positions have been averaged (Fig. 6, upper panel). In the model, the total flux is forced to be equal to that measured in the map (i.e. 1.22 Jy × km s^{-1}). We set the central velocity at 28.8 km s^{-1}. The results are summarized in Table 1. In this simulation, the temperature and the velocity are constant inside r_1 (resp. 20 K and 4.2 km s^{-1}). The shock at r_1 decreases the velocity (increases the density) by a factor of 3.9 and the temperature rises to 530 K (Figs. 7 and 8). Then, inside the region of compressed matter (between r_1 and $r_{\rm f}$), the temperature decreases to ∼175 K. The physical conditions between $r_{\rm f}$ and r_2 are in fact not constrained either by our model or by the data at 21 cm, and in Table 1 they are only extrapolated (for more details, see Libert et al. 2007).

The model assumes that the H I emission is optically thin ($\tau \ll 1$). This can be verified using the output column density profile (Fig. 8, right panel) and the expression

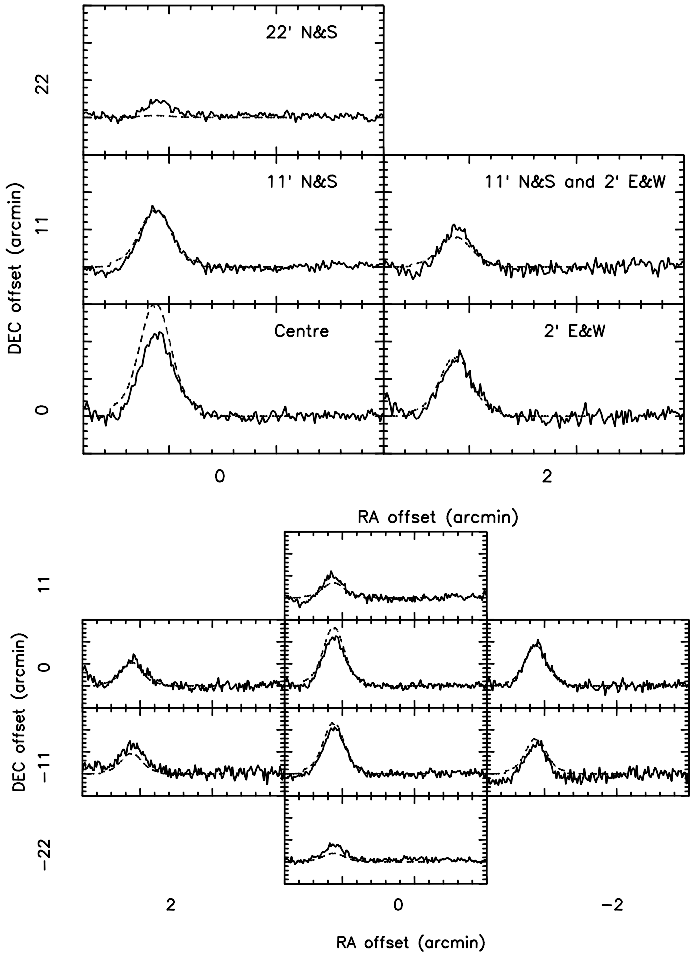

Fig. 6. H I observations vs. model (dashed line): *the upper panel* shows the model discussed in Sect. 5 and compared to a symmetrized H I map of RX Lep. *The lower panel* presents the same model shifted by 4.4′S and 0.4′W and compared to the H I map of RX Lep (as in Fig. 4).

$\tau = 5.50 \times 10^{-19} \frac{N_{\rm H}}{T \Delta V}$ (Eq. (12), Libert et al. 2007) where $N_{\rm H}$ is in cm^{-2} and ΔV, the line width, in km s^{-1}. With $T > 175$ K and $\Delta V \sim 3.8$ km s^{-1}, the optical depth stays below 0.5 at all impact parameters >0.1′ from the central star.

In general, the model provides a satisfactory fit to the symmetrized H I spectra that we have obtained on RX Lep. However, it predicts a flux above the observations on the central position and below at 22′ in declination. This can be understood as a consequence of the 4.4′ offset to the south noted in Sect. 4. By moving the model 4.4′ south and 0.4′ west with respect to the central star, we can improve the fit to the observed data (Fig. 6, lower panel). This gives support to the offset values that we have determined by Gaussian-fitting in Sect. 4. Yet, the spectrum on the position at 22′ south is not well reproduced, suggesting that the source is more extended along the north-south direction than along the east-west one, as suspected in Sect. 4.

In the past (Y CVn, Libert et al. 2007), we already attempted to better fit the data by a shift in position to take into account the deformation of the envelope by the ISM. However, this approach is artificial because we used a spherical model that is not centered on the star position. It is only meant to illustrate the need for an H I mapping of this interesting source with a better spatial resolution and the need to develop a true non-spherical modeling of detached shells.

Table 1. Model parameters (d = 137 pc), with notations the same as in Libert et al. (2007).

$\dot{M}$ (in hydrogen)	1.27×10^{-7} $M_\odot$ yr^{-1}
μ	1.3
t_1	5 927 years
$t_{\rm DS}$	36 800 years
r_1	2.55×10^{-2} pc (0.64′)
$r_{\rm f}$	3.67×10^{-2} pc (0.92′)
r_2	4.58×10^{-2} pc (1.15′)
$T_0(\equiv T_1^-)$, T_1^+	20 K, 528 K
$T_{\rm f}$ (= T_2)	175 K
$v_0(\equiv {\rm v}_1^-)$, ${\rm v}_1^+$	4.2 km s^{-1}, 1.07 km s^{-1}
$v_{\rm f}$	0.16 km s^{-1}
v_2	1.2 km s^{-1}
n_1^-, n_1^+	148 H cm^{-3}, 578 H cm^{-3}
$n_{\rm f}^-$, $n_{\rm f}^+$	2.1×10^3 H cm^{-3}, 2.5 H cm^{-3}
n_2	1.3 H cm^{-3}
$M_{r<r_1}$ (in hydrogen)	0.75×10^{-3} $M_\odot$
$M_{\rm DT,CS}$ (in hydrogen)	4.67×10^{-3} $M_\odot$
$M_{\rm DT,EX}$ (in hydrogen)	0.010×10^{-3} $M_\odot$

6. Discussion

RX Lep shows evidence of a circumstellar envelope of ∼0.01 $M_\odot$ that may be the result of its stellar wind decelerated by the external medium. This star is an oxygen-rich, semi-regular variable on the E-AGB (no evidence of Tc, cf. Sect. 2). It is in the same evolutionary stage as EP Aqr and X Her, which have also been detected in H I and for which the emission at 21 cm shows evidence of significant circumstellar envelopes (Le Bertre & Gérard 2004; Gardan et al. 2006). We note that these 3 stars share the same variability properties and have about the same luminosity (∼4500 $L_\odot$) and the same effective temperature (∼3200 K). It suggests that mass loss can already occur efficiently for this type of star on the E-AGB.

Our model strongly relies on the mass-loss rate estimated from CO observations. It is noteworthy that this estimate is consistent with Reimers' relation (Reimers 1978). Indeed, by adopting $M \sim 3$ $M_\odot$, $L \sim 4500$ $L_\odot$ and $T_{\rm eff} \sim 3300$ K (Sect. 2), this relation gives $\dot{M} \sim 2 \times 10^{-7}$ $M_\odot$ yr^{-1}. However, the luminosity was probably lower in the past, as was the mass-loss rate. This suggests that the age (42 700 years) is underestimated.

The model and our observations together put constraints on the physical conditions within the CS between the termination shock (r_1) and the interface ($r_{\rm f}$). Directly from the observations, the mean temperature should be $\lesssim$300 K. Based on the assumption of an adiabatic shock at r_1, it implies an increase in temperature to ∼500 K. Thus, the gas must be cooled down in the CS. Estimating the cooling rate is difficult at such low temperatures. Nevertheless, the H I line-profiles put constraints on the behavior of the temperature because it is coupled to the kinematics (Libert et al. 2007). The temperature profile shown in Fig. 7 (lower panel) yields the best fit to the shape of the H I spectra. Between $r_{\rm f}$ and r_2, our model has only been extrapolated. This region is probably dominated by interstellar material flowing at ∼50 km s^{-1} through the bow shock. The material should be denser than assumed in our model; indeed, this region is fed by the interstellar medium that has been swept up through the relative motion of RX Lep circumstellar shell, at ∼50 km s^{-1}, rather than by the expansion of the shell during the same period of 4×10^4 years. Also it is expected to be ionized, and therefore might not contribute significantly to the H I emission that we detected.

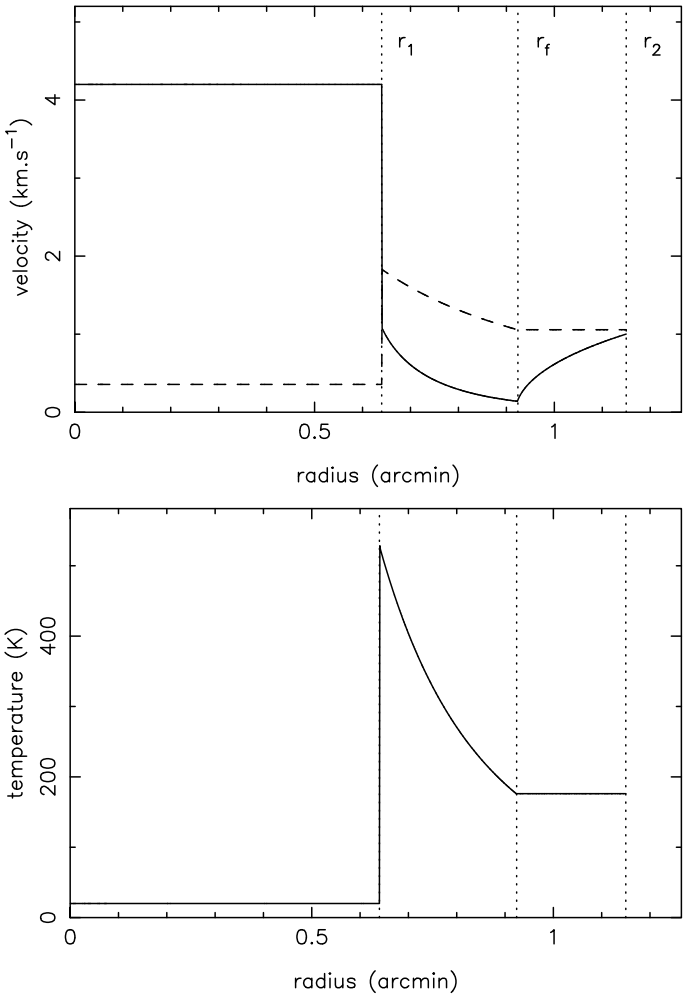

Fig. 7. *Upper panel*: velocity profile. The dashed line represents the isothermal sound velocity. *Lower panel*: temperature profile adopted for the model.

The H I data indicate that RX Lep's CS is offset about 4′ to the south and 0.5′ to the west. This agrees within 25° with the direction of the proper motion given by Hipparcos (PA ∼ 31°). In addition, the model hints that the shell is not completely spherical, and that RX Lep is slightly elongated mostly in the N/S direction. This suggests that the elongated shape observed in H I is connected to the motion of RX Lep through the local ISM. Villaver et al. (2003) have made numerical simulations of the evolution of a low-mass star moving supersonically through the ISM and find that, due to the ram-pressure stripping, most of the mass ejected during the AGB phase is left downstream. The left panel in their Fig. 1 shows that CSs are progressively distorted and become elongated in the direction of the motion with respect to their surrounding ISM. The 25° difference between the space motion of the star and the elongation of the shell could then be due to the intrinsic velocity of the ISM local to RX Lep relative to the LSR. Such intrinsic motions are currently found in the local solar neighborhood (Redfield & Linsky 2008, Fig. 16 and references therein). A significant fraction of the velocity of the local ISM is a reflection of the solar motion; nevertheless, the velocity of the Sun with respect to the LSR (13.4 km s^{-1}, according to Dehnen & Binney 1998) is 25° away from the direction of the velocity of the average local ISM with respect to the Sun (26.7 km s^{-1}).

It is also worth noting that for RX Lep there is no significant difference between the H I and CO central velocities, as if the interaction only occurs in the plane of the sky.

We have examined the IRAS maps that have been reprocessed recently by Miville-Deschênes & Lagache (2005, IRIS: Improved Reprocessing of the IRAS Survey). The 60 μm and 100 μm images (Fig. 9) suggest a small extended source ($\phi \sim 6'$–$8'$). The source at 100 μm might be shifted by ∼2′ to the south. There is also an extension (∼12′) to the south; however, it might be an artifact due to the satellite scanning in the north-south direction. In these images, we cannot confirm the X0509-119 offset with respect to RX Lep (cf. Sect. 2). New data with a better spatial resolution, e.g. from the Far Infrared All-Sky Survey of Akari, may help to clarify this situation.

In their H I survey of evolved stars, Gérard & Le Bertre (2006) found that the line-profiles are Gaussian-shaped and often offset with respect to the stellar velocity by ∼1–3 km s^{-1} towards 0 km s^{-1} LSR. Several H I sources were also noted to be spatially offset from the central star. They suggest that these effects could be related to a non-isotropic interaction with the local ISM. Matthews & Reid (2007) have imaged the H I emission around RS Cnc with the VLA. They find that it is elongated with a peak on the stellar position and a filament extending ∼6′ to the northwest, in a direction opposite to that given by the proper motion. Recently, Matthews et al. (2008) have imaged the H I emission of Mira with the VLA. As for RS Cnc, they find a "head-tail" morphology oriented along the star proper motion and consistent, on large scales, with the far-ultraviolet emission discovered by GALEX (Martin et al. 2007). Furthermore, the high spectral resolution H I data obtained with the NRT along the 2-degree GALEX trail reveal a deceleration of the gas caused by interaction with the local ISM. Finally, using Spitzer MIPS data obtained on R Hya at 70 μm, Ueta et al. (2006) discovered a bow-shock structure *ahead* of the star in the direction of its motion. The excess emission that delineates this bow shock is seen at 70 μm, but not at 160 μm; it may partly come from the [O I] cooling line at 63 μm. Although we have presently no direct evidence in H I of a bow-shock, both structures, bow-shock and H I trail, should be causally related (Wareing et al. 2006). In fact, as the velocity of these sources with respect to the ISM is often high (see e.g. Nyman et al. 1992 or Mennessier et al. 2001), the interstellar material is probably ionized through the bow shock, so that we may never detect directly such a bow-shock structure in H I at 21 cm. Better tracers would likely be line emission in the UV/optical/IR ranges (H_α, [Fe II], [O I], etc.).

We therefore have a convergent set of results that shows that AGB stars are associated with large-scale circumstellar shells distorted by the motion of these evolved objects through the ISM (Villaver et al. 2003). We suggest that RX Lep is one more source in such a case. That the source is elongated in the same direction as its offset and nearly opposite to the direction of motion, argues in favor of a head-tail morphology.

7. Conclusions

We detected CO(2–1) and H I line emissions from the semi-regular oxygen-rich E-AGB star, RX Lep. These emissions indicate a stellar outflow at a velocity ∼4.2 km s^{-1} and a rate $\sim 1.7 \times 10^{-7}$ $M_\odot$ yr^{-1}, with a duration of 4×10^4 years. The H I source has a size of ∼2′ (≈0.08 pc) in the east-west direction and possibly 15′ (≈0.6 pc) in the north-south direction.

The modeling of the H I line profiles obtained at different positions suggests that the outflow is slowed down by the interaction with the ambient ISM, and that the external part of RX Lep

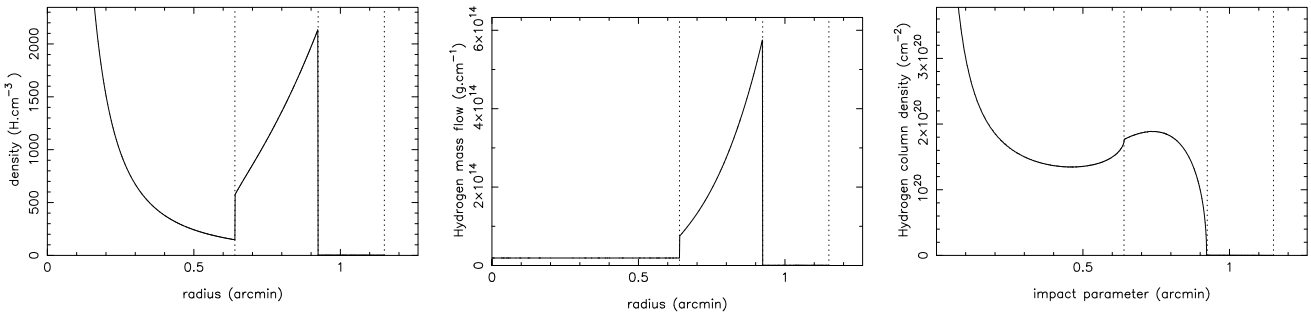

Fig. 8. *Left panel*: atomic hydrogen density profile. *Center panel*: atomic hydrogen mass-flow profile. *Right panel*: atomic hydrogen column density calculated by the model. The vertical dotted lines show the radii, r_1, r_f and r_2, used in the model.

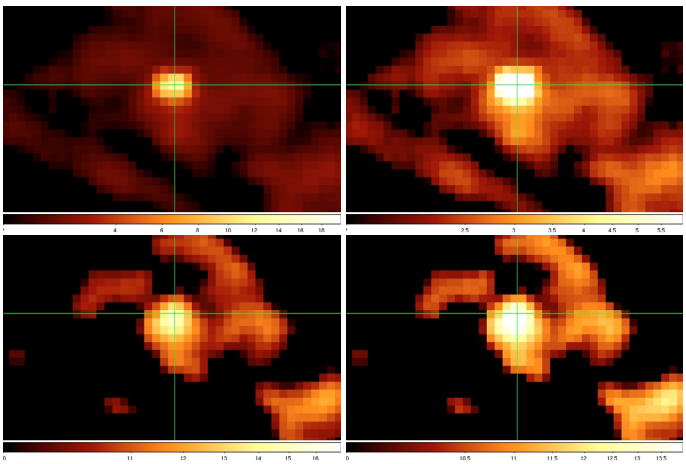

Fig. 9. Reprocessed IRAS images (IRIS) at 60 μm (*upper panels*) and 100 μm (*lower panels*). To enhance the suspected extended emission to the south, we present a non-saturated version (*left*) and a saturated one (*right*) for both wavelengths. The field is ~65′ × 39′ and the green reticles mark the position of RX Lep (north is to the top and east to the left).

circumstellar shell is made of compressed material, at ~200 K, as in the well-known detached shell around Y CVn.

The elongated shape of the RX Lep H I source is compatible with the direction of its proper motion, as in the cases of Mira and RS Cnc, which have already been studied at high angular resolution with the VLA.

Acknowledgements. The Nançay Radio Observatory is the Unité scientifique de Nançay of the Observatoire de Paris, associated as Unité de Service et de Recherche (USR) No. B704 to the French Centre National de la Recherche Scientifique (CNRS). The Nançay Observatory also gratefully acknowledges the financial support of the Conseil Régional de la Région Centre in France. This research made use of the SIMBAD database, operated at the CDS, Strasbourg, France, and of the NASA's Astrophysics Data System. We thank the referee, Dr T. Ueta, and Dr L. Matthews for helpful suggestions.

References

Booth, R. S., Delgado, G., Hagström, M., et al. 1989, A&A, 216, 315
Cristian, V.-C., Donahue, R. A., Soon, W. H., Baliunas, S. L., & Henry, G. W. 1995, PASP, 107, 411
Dehnen, W., & Binney, J. J. 1998, MNRAS, 298, 387
Dumm, T., & Schild, H. 1998, New Astron., 3, 137
Epchtein, N., Le Bertre, T., Lépine, J. R. D., et al. 1987, A&AS, 71, 39
Fouqué, P., Le Bertre, T., Epchtein, N., Guglielmo, F., & Kerschbaum, F. 1992, A&AS, 93, 151
Gardan, E., Gérard, E., & Le Bertre, T. 2006, MNRAS, 365, 245
Gérard, E., & Le Bertre, T. 2006, AJ, 132, 2566
Glassgold, A. E., & Huggins, P. J. 1983, MNRAS, 203, 517
Habing, H. 1996, A&AR, 7, 97
Hrivnak, B. J., & Bieging, J. H. 2005, ApJ, 624, 331
Hrivnak, B. J., Kwok, S., & Su, K. Y. L. 2001, AJ, 121, 2775
IRAS Science Team 1988, IRAS Catalogs and Atlases, NASA RP-1190, Vol. 7
Izumiura, H., Hashimoto, O., Kawara, K., Yamamura, I., & Waters, L. B. F. M., 1996, A&A, 315, L221
Kerschbaum, F., & Olofsson, H. 1999, A&AS, 138, 299
Knapp, G. R., & Morris, M. 1985, ApJ, 292, 640
Kukarkin, B. V., Kholopov, P. N., Pskovsky, Y. P., et al. 1971, General Catalogue of Variable Stars, 3rd edn.
Lafon, J.-P. J., & Berruyer, N. 1991, A&ARv, 2, 249
Lamers, H. J. G. L. M., & Cassinelli, J. P. 1999, Introduction to Stellar Winds, (Cambridge: Cambridge University Press)
Leão, I. C., de Laverny, P., Mékarnia, D., De Medeiros, J. R., & Vandame, B. 2006, A&A, 455, 187
Le Bertre, T., & Gérard, E. 2004, A&A, 419, 549
Le Bertre, T., Matsuura, M., Winters, J. M., et al. 2001, A&A, 376, 997
Lebzelter, Th., & Hron, J. 1999, A&A, 351, 533
Libert, Y., Gérard, E., & Le Bertre, T. 2007, MNRAS, 380, 1161
Little, S. J., Little-Marenin, I. R., & Bauer, W. H. 1987, AJ, 94, 981
Mamon, G. A., Glassgold, A. E., & Huggins, P. J. 1988, ApJ, 328, 797
Martin, D. C., Seibert, M., Neill, J. D., et al. 2007, Nature, 448, 780
Matthews, L. D., & Reid, M. J. 2007, AJ, 133, 2291
Matthews, L. D., Libert, Y., Gérard, E., Le Bertre, T., & Reid, M. J. 2008, ApJ, 684, 603
Mauron, N., & Huggins, P. J. 2000, A&A, 359, 707
Mennessier, M. O., Mowlavi, N., Alvarez, R., & Luri, X. 2001, A&A, 374, 968
Miville-Deschênes, M.-A., & Lagache, G. 2005, ApJS, 157, 302
Nyman, L.-Å., Booth, R. S., Carlström, U., et al. 1992, A&AS, 93, 121
Olofsson, H. 1999, Asymptotic Giant Branch Stars, ed. T. Le Bertre, A. Lèbre, & C. Waelkens, IAU Symp., 191, 3
Olofsson, H., Bergman, P., Lucas, R., et al. 2000, A&A, 353, 583
Olofsson, H., González Delgado, D., Kerschbaum, F., & Schöier, F. L. 2002, A&A, 391, 1053
Paschenko, M., Slysh, V., Strukov, I., et al. 1971, A&A, 11, 482
Pety, J. 2005, in SF2A-2005: Semaine de l'Astrophysique Française, ed. F. Casoli, T. Contini, J. M. Hameury, & L. Pagani, 721
Ramstedt, S., Schöier, F. L., Olofsson, H., & Lundgren, A. A. 2008, A&A, 487, 645
Redfield, S., & Linsky, J. L. 2008, ApJ, 673, 283
Reimers, D. 1978, A&A, 67, 161
Renzini, A. 1981, in Physical processes in Red giants, ed. Jr. Iben I., & A. Renzini, (D. Reidel), 431
Samus, N. N., Durlevich, O. V., et al. 2004, Combined General Catalog of Variable Stars, ed. 4.2 (Moscow: Sternberg Astron. Inst.)
Schröder, K.-P., Winters, J. M., & Sedlmayr, E. 1999, A&A, 349, 898
Simis, Y. J. W., Icke, V., & Dominik, C. 2001, A&A 371, 205
Soker, N. 2002, ApJ, 570, 369
Ueta, T., Speck, A. K., Stencel, R. E., et al. 2006, ApJ, 648, L39
Villaver, E., García-Segura, G., & Manchado, A. 2003, ApJ, 585, L49
Wareing, C. J., Zijlstra, A. A., Speck, A. K., et al. 2006, MNRAS, 372, L63
Wareing, C. J., Zijlstra, A. A., & O'Brien, T. J. 2007, MNRAS, 382, 1233
Wilson, R. E. 1953, General Catalogue of Stellar Radial Velocities, Carnegie Inst. Washington D. C. Publ., 601
Winters, J. M., Le Bertre, T., Jeong, K. S., Helling, Ch., & Sedlmayr, E. 2000, A&A, 361, 641
Winters, J. M., Le Bertre, T., Jeong, K. S., Nyman, L.-Å., & Epchtein, N. 2003, A&A, 409, 715
Young, K., Phillips, T. G., & Knapp, G. R. 1993, ApJ, 409, 725